8-1-2012

Influence of Solvent on the Chiral Resolution of Organic Molecules on Au(111): EC-STM Study of Biphenyl Dicarboxylic Acid on Au(111) in an Aqueous Environment

Byung I. Kim
Boise State University

Joey Hanson
Boise State University

Matthew Turner
Boise State University

Lauren Reeder
Boise State University

Influence of Solvent on the Chiral Resolution of Organic Molecules on Au(111): EC-STM Study of Biphenyl Dicarboxylic Acid on Au(111) in an Aqueous Environment

Byung I. Kim, Joey Hanson, Matthew Turner, and Lauren Reeder

Department of Physics, Boise State University, Boise ID 83725-1570

Abstract

Adsorption-induced chiral resolution of organic molecules is important due to its potential applications in stereo-selective catalysis. We studied the adsorption-induced chiral resolution using a model achiral molecule of 4,4' biphenyl dicarboxylic acid (BPDA) on Au(111) in 0.1 M perchloric acid (HClO4) by electrochemical scanning tunneling microscopy (EC-STM). Our experimental data showed that the BPDA molecules formed island structures with distinctive preferred orientations at the length scale of the molecular size. The molecules did not show any orientational ordering above the length scale, indicating that chiral resolution was absent in the aqueous environment. Previously, the molecules were found to have chiral resolution on Au(111) in ultra-high vacuum conditions (UHV). We calculated angle-dependent binding energy between the substrate and a BPDA molecule, the intermolecular interactions between the BPDA molecules, and their interactions with water molecules. The calculations suggest that the absence of chiral resolution in the aqueous environment originated from the decrease in the intermolecular energy of the BPDA molecules due to their hydrogen bonds with the surrounding water molecules. The strength of the hydrogen bonding between BPDA molecules was sufficient to overcome the energy barrier for chiral resolution through rotational motion in UHV, but not in an aqueous environment.

Keywords: adsorption induced chirality; EC-STM; 4,4' biphenyl dicarboxylic acid; hydrogen bond; binding energy.

*Corresponding author. E-mail: byungkim@boisestate.edu

Introduction

Two-dimensional (2D) stereo-selectivity using chiral surface processes and reactions has been conceived as an efficient method of stereo-control in the production of single-enantiomer compounds for pharmaceutical applications [1,2], including the use of enantiomeric drugs to target enzymes, hormones, and receptors on cell surfaces, along with other compounds that are made up of chiral amino acids, carbohydrates, and lipids [1,3]. While one enantiomeric form is effective in drugs, others can cause toxicity in some cases [4]. The creation of 2D chiral surfaces has attracted much attention from researchers due to its importance in these applications. This has been demonstrated in a variety of both chiral and achiral compounds, including various amino acids [5-7], benzoic acid [8], tartaric acid [9], and others [10-13]. When an achiral molecule adsorbs to an achiral metal surface, chirality is known to be induced by the adsorption of organic molecules [14-21]. The adsorption-induced chirality has been reported in a self-assembled monolayer of discotic liquid crystal [18], in the adsorption of single strand DNA [19], in enantiomorphous domains from arachidic anhydride [20], and in the dimerization of adsorbed cysteine [21].

Due to the potential applications in stereo-selective catalysis, the adsorption-induced chirality has been studied in a variety of systems to resolve chiral domains [10,14-23]. The chiral resolution could possibly be driven by molecular recognition based on the combination of adsorbate-substrate interaction and intermolecular interaction [10,23]. For example, it has been revealed that chiral resolution occurs for the asymmetric planar molecule 4-trans-2-(pyrid-4-yl-vinyl) benzoic acid (PVBA) on fcc(111) metal surfaces and is strongly dependent not only on the interaction between adsorbates, but also on the interaction between the substrate and the adsorbate [10,24]. Adsorption configuration of PVBA on fcc(111) dictates the intermolecular interaction energy between different chiral species. On Pd(111) there is no difference in intermolecular interaction energy between chiral species, whereas on Ag(111) there is an intermolecular energy difference for heterochiral molecular combination. In another approach, Stepanow et. al. reported that while symmetric 4,4’ biphenyl-dicarboxylic acid (BPDA) molecules organize in networks on Cu(100) in an ultra-high vacuum (UHV), asymmetric stilbene

dicarboxylic acid molecules experience mesoscopic chiral resolution, demonstrating the effect of molecular symmetry on chirality [25]. Chiral resolutions were also observed for smaller organic molecules on metal surfaces in the electrochemical environment [26-28]. These studies suggest that molecular size also appears to be an important factor in determining chiral resolution. In this paper, we studied the solvent's effect on chiral resolution between BPDA molecules on Au(111) using electrochemical scanning tunneling microscopy (EC-STM). A previous STM study reported that the BPDA molecules formed ordered chiral domains on Au(111) in UHV [11], although both BPDA and Au(111) are achiral. The electrochemical environment was used as a means to modulate the strength of intermolecular interaction through the involvement of water molecules in addition to the existing adsorbate-substrate interaction.

Material and Methods

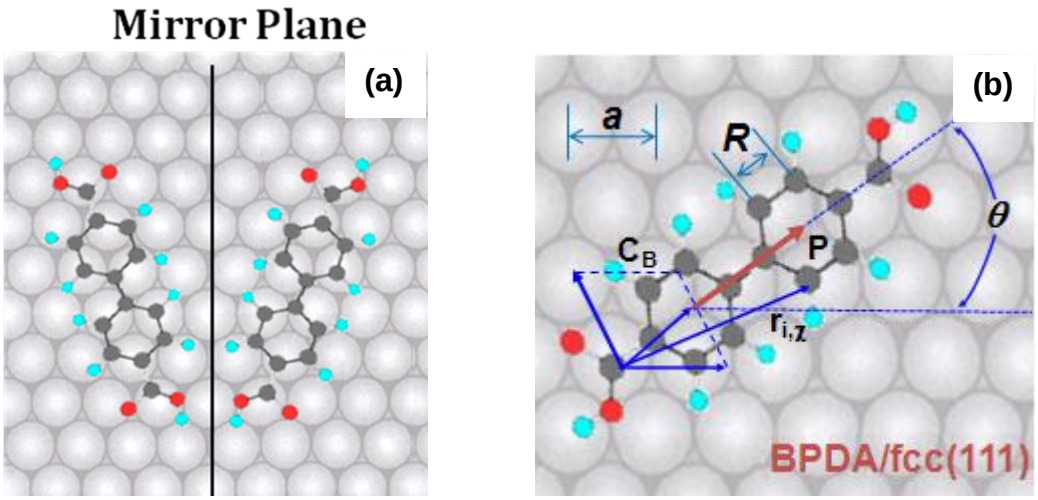

Figure 1. (a) Structural model of BPDA on Au(111). When a BPDA molecule is adsorbed on fcc(111), the composite structure of BPDA on fcc (111) is chiral, because the composite structure cannot be overlapped with its mirror image. (**b)** Molecular configuration and relevant parameters were used to calculate the binding energy potentials with a model potential developed between a carbon atom and the Au(111) surface. Each potential value was added for all carbon atoms of two aromatic rings. *R*: aromatic ring radius; *a*: surface lattice constant of fcc(111); $\vec{C}_B$: the center vector of the benzoic ring; $\vec{P}$: the vector from the center of one benzoic ring to the center of the other; θ: the angle between the $\vec{P}$ vector and the direction of an atomic row.

A BPDA molecule is composed of two benzene rings flanked by two carboxylic acid groups at opposite ends of the molecule. Because each aromatic ring of BPDA is symmetric with respect to the

molecular axis, there is no chiral angle as shown in Figure 1a. The molecule has D_{2D}-symmetry in three dimensions but becomes a C_{2v}-symmetric molecule upon adsorption to the metal surface due to the removal of the horizontal mirror-plane [29].

The EC-STM used in this study was a Nanoscope E (Digital Instruments, Santa Barbara, CA). Imaging was carried out in a solution of 0.1 M HClO4 and ~1mM BPDA under ambient conditions. The tip required for the EC-STM was made from a tungsten (W) wire via an electrochemical etching process using 2 M KOH and a power supply as a source of electrical current. This tip was then covered with nail polish for insulation, except the very end of the tip, to allow current to flow between the surface and the tip. The gold sample surfaces were prepared and attached to the fluid cell. The gold surface was produced by flame annealing the end of a pure gold wire (1.0 mm diameter) until a small bead formed (3.5 mm diameter). Cyclic voltammograms were used to prepare the gold sample surface through reduction and oxidation processes in a scan range of 0 V to 1 V. A fluid cell was designed and developed to receive voltages from an electrometer through a potentiostat. The controller recorded the current between the working (sample), counter (platinum), and reference (metallic silver) electrodes as the working electrode potential was ramped linearly. The supporting electrolyte in this system was 0.1 M perchloric acid ($HClO_4$) (Acros, Geel, Belgium). The BPDA was purchased from Sigma (St. Louis, MO) and was dissolved in H_2O overnight to form a saturated solution with a concentration of ~1 mM. The molecular structure of the achiral molecules was imaged on the surface in the presence of 0.1 M $HClO_4$ at room temperature using the EC-STM. The images shown here were obtained in the constant-current mode to measure the height of the BPDA molecules on the Au(111) surface.

We interpreted the observed EC-STM data based on our previous model involving PVBA on Pd(111) and Ag(111) in UHV [10,23]. This model was capable of explaining the chiral resolution of structures constructed by molecules with two anchoring points to a substrate such as PVBA on fcc(111) and R,R-tartaric acid on Cu(110) [30]. Figure 1b shows the molecular adsorption of BPDA on the fcc (111) surface for the binding energy calculation. The experimentally observed orientations of BPDA molecules on Au(111) were analyzed by calculating the binding energy as a function of angle θ between

the horizontal axis and the P-vector that extends from the middle of one benzoic ring to the other, based on our previous model potential for PVBA on fcc(111) [10]. In this model, each aromatic ring is considered a hexagon with equal bonding length R as a first-order approximation. To make a carbon atom of the aromatic ring prefer the top site of a substrate atom, the model potential is designed to have a minimum at the top site and a maximum at a hollow site of metal atoms on the substrate. Each potential value was added for all carbon atoms of two aromatic rings to calculate the relative binding energy $E(\vec{C}_B, \vec{P})$ of BPDA on Au(111) given a center vector of the benzoic ring $\vec{C}_B$, and a given vector $\vec{P}$ from the center of the benzoic ring to the center of the other. The relative binding energy $E(\vec{C}_B, \vec{P})$ was then minimized for a given orientation within a unit cell, shown as a parallelogram in Figure 1b. This calculation was repeated for every angle θ from 0° to 180° for R/a ratios ranging from 0.4422 to 0.5275.

Results and Discussion

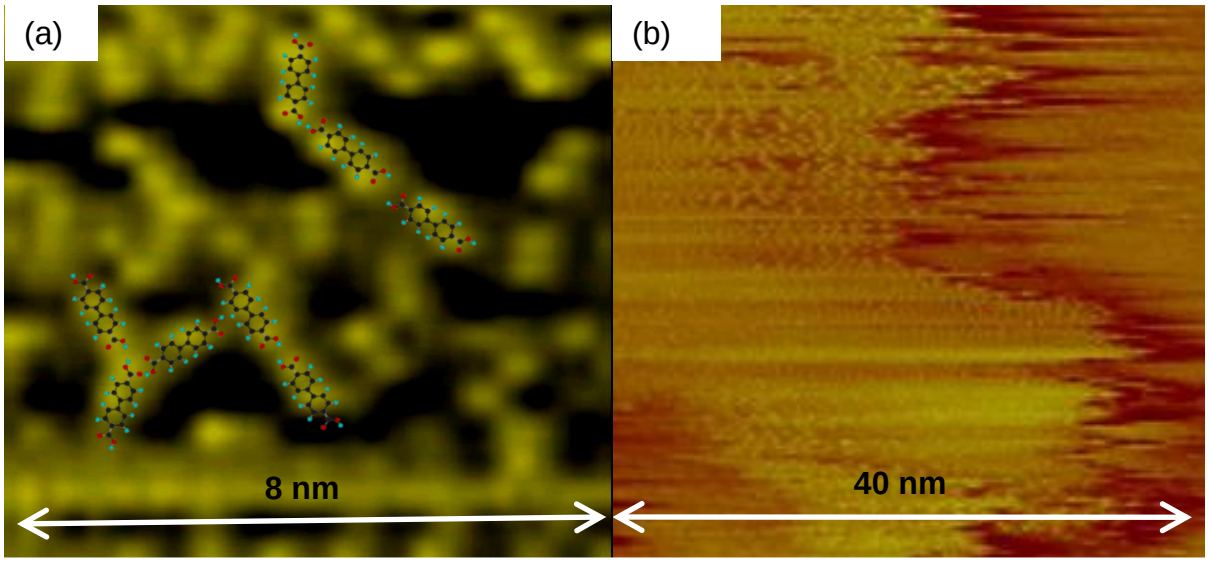

Figure 2. STM images of BPDA on Au(111) in 0.1 M $HClO_4$. (**a**) The structural configurations of the intermolecular bonding of BPDA molecules on Au(111) collected in 0.1 M $HClO_4$ and viewed in a 8nm x 8nm window. Overlaid in the figure are representative molecular structures of BPDA. Trimeric and dimeric hydrogen bonding motifs are visible. Ordered structures were not observed in scans of 0.1M $ClO4^-$ in the absence of BPDA (not shown). (**b**) The structural configurations of adsorbed BPDA molecules on Au(111) collected in 0.1 M $HClO_4$ and viewed in 40 nm x 40 nm window. The molecular surface of Au(111) is visible on the right hand side and in the bottom left hand corner.

EC-STM imaging *in situ* in Figure 2a shows a typical EC-STM image with "peanut-like" molecular structures adsorbed on Au(111). When the structures are compared with the BPDA skeleton, each peanut-like structure can be related to a single BPDA molecule, as shown in Figure 2a. The peanut-like image may appear larger than the model because the tunneling current can cause diffusion of the image. This type of diffusive effect of the tunneling current on the EC-STM image has been reported previously [10,31]. Each lobe shape of an individual molecule is associated with a phenyl ring, as the molecules adopt a flat configuration due to the π-d interaction between the BPDA and Au atoms based on previous reports [10,23,31,32]. It is important to note that each water molecule could not be observed in the EC-STM images since water is less conductive than the BPDA molecules. The limited EC-STM resolution in the aqueous environment appeared to be related to the interference of water molecules with the BPDA molecules. In the UHV environment, higher resolution could be achieved due to the absence of interference from other molecules in the medium.

A larger scale EC-STM image, Figure 2b, shows that BPDA molecules were observed to form a self-assembled large island structure greater than 100 nm in length. Interestingly, highly ordered arrays were not observed within the island structure, unlike those previously shown in UHV conditions [11]. Zhu et al. observed that BPDA molecules form well-ordered arrays due to hydrogen bonds between carboxyl groups of adjacent molecules on Au(111) [11]. The observed arrays in UHV had straight edges, indicating growth occurred in a concerted direction. In the present study, the self-assembled structures had jagged-edge regions (see Figure 2b), which suggests that local distinctive orientations were favorable over simple directional growth observed in UHV. Monomers were not observed away from the island, showing that they were unstable as individuals on the Au(111) surface, both in UHV and in a solution. These results indicate that the BPDA molecules were sufficiently mobile in translational motion to form island structures.

Each molecule appears to orient in a certain preferred direction in relation to the Au(111) substrate although the molecular structures do not have long-range ordered arrays, as shown in Figure 3a. The orientations of each BPDA molecule in Figure 3a were quantitatively analyzed using fast

Fourier transform (FFT). In the FFT of the image (Figure 3b), the darker spots on the figure represent higher occurrences of each angle, while white areas indicate lower frequency or non-existent orientations. There is a trend in the distribution of the relative angles with which BPDA adsorbs to Au(111). The solid lines coincide with the direction of the atomic rows, whereas the dashed lines show the direction of common BPDA orientations. The atomic orientation of Au(111) is six-fold, creating repetitive intervals of 60 degrees. Figure 3b indicates that the angle orientation of BPDA molecules occur $\pm 17^0$ from the 30^0 axis in relation to the metal substrate. The result confirms that each molecule has a certain directional preference on the Au(111) substrate.

The FFT of the image also contains information on the length scale of molecular arrangement as well as orientations. Figure 3c illustrates a sectional profile along the 347^0 axis of Figure 3b. Each peak represents the periodic features from the original EC-STM image (Figure 3a). The peak position in the horizontal $k/2\pi$ axis allows us to calculate the length scale (p) with $p = 2\pi/k$. A length scale of 2nm was determined based upon the relative positions of the peaks in the sectional profile, $\pm 4.6\times10^8$ m^{-1}. As expected, this length scale corresponds roughly to the combined length of the molecular size (~1 nm) and intermolecular gap. This result indicates that the BPDA molecules formed island structures with distinctive preferred orientations at the length scale of the molecular size. However, the molecules did not exhibit any orientational ordering beyond the molecular length scale, confirming that chiral resolution is absent in the aqueous environment. This short length in orientation order suggests that the close proximity of molecules was not enough to induce ordered arrays. Considering that the hydrogen bond groups were parallel with the long axis of the BPDA molecules (see Figure 1a), the intermolecular interaction did not appear to be fully optimized in the observed island structure in the electrochemical environment. Because the rotational motion was necessary to form an ordered structure through the optimized hydrogen bonds, the absence of ordered arrays proposes that the monomers were considerably less rotatable in the aqueous phase than monomers in vacuum.

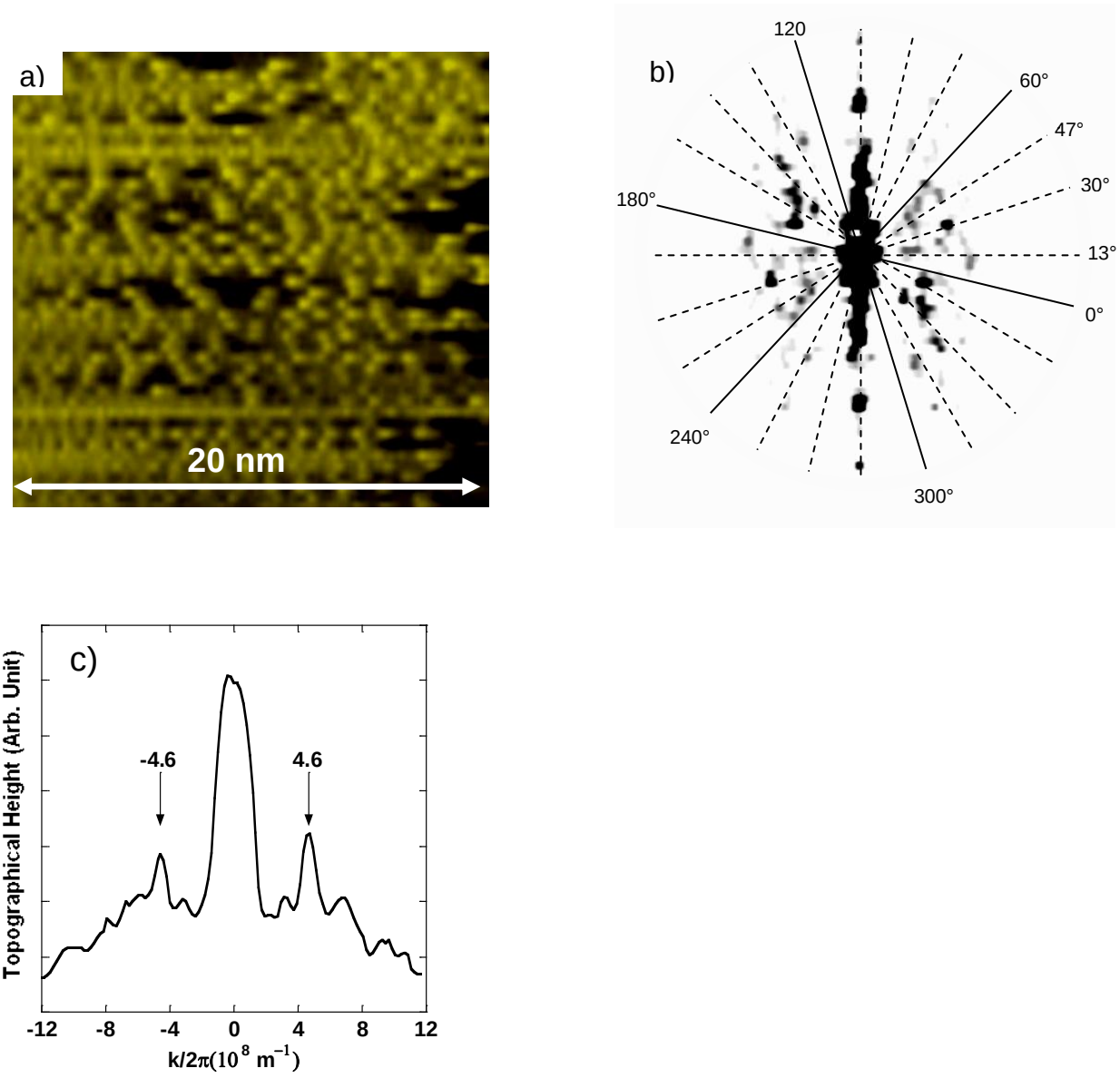

Figure 3 (a) STM image of BPDA molecules adsorbed onto Au(111) in 0.1 M $HClO_4$ **(b)** FFT of the image, each peak represents a higher instance of molecule distributions for each angle. The solid lines represent the direction of the atomic rows of Au(111). The dashed lines are generated from the dark areas and approximate the orientation of the BPDA molecules. **(c)** A sectional profile along the 347^0 direction. The peaks marked with arrows represent the periodic features of the STM image. The length scale was calculated to be 2 nm based on the position of the peaks, $\pm 4.6\times10^8$ m^{-1}.

The observed distinctive preferred orientations lead to our earlier model of PVBA on fcc(111) surfaces [10,23], which explains the orientations as due to the interaction between the adsorbed molecules and the substrate lattice. We calculated the binding energy curve as a function of its orientation for the angle range 0° to 180° using the method presented in our section for Materials and Methods. The curve has 60° periodicity, as expected with the six-fold symmetry of the Au(111) surface.

The ratio R/a is a parameter that represents different substrates. In this calculation, we used a surface lattice constant of 2.75 Å instead of 2.87 Å for Au(111) based on the 4% contraction of atomic spacing during Au reconstruction [33,34]. In contrast to the angle-dependent binding energy calculations reported for PVBA on Pd(111) [10], the binding energy of BPDA on Au(111) is symmetric around 30°, 90°, and 150º. This energy symmetry is due to the symmetry of the composite structure of BPDA with the Au(111) surface at the angles of 30°, 90°, and 150º (for example, the composite structure shown in Figure 4b, has symmetry along the 30° axis). In Figure 4a, the minimum binding energies occur at 13°, 30° and 47° with respect to an atomic row on the substrate as marked with arrows. These angles match the experimentally observed intervals ± 17^0 from the 30^0 axis shown in Figure 3b, confirming that the molecular orientations originate from the binding interactions of BPDA on Au(111).

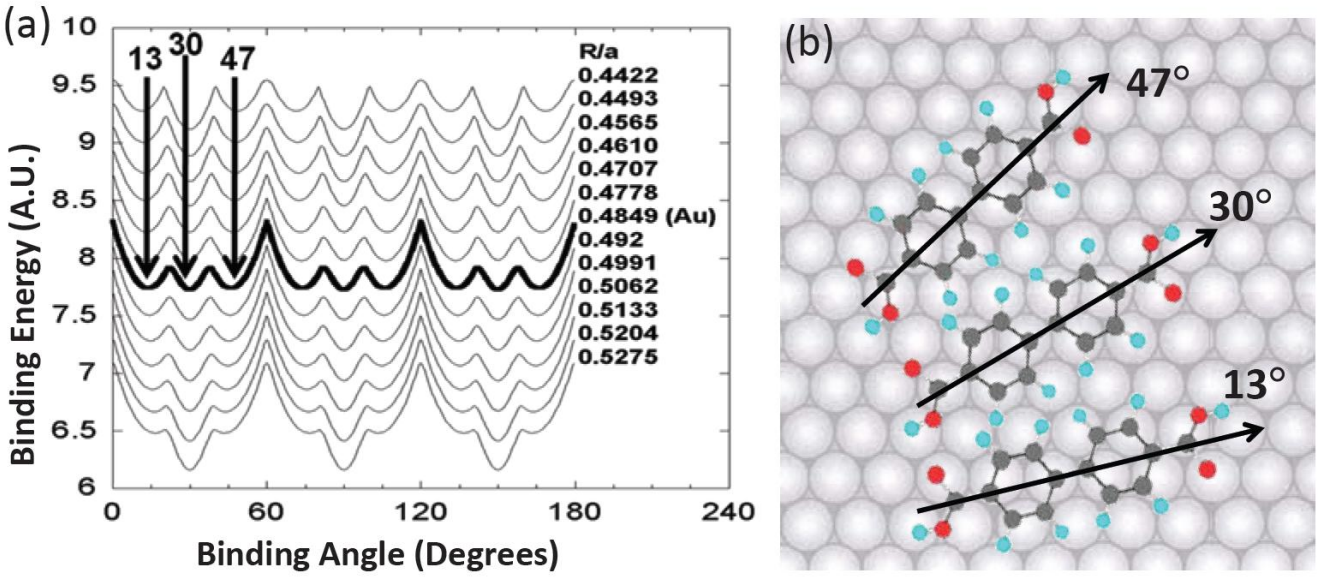

Figure 4. (a) Theoretical binding energy calculations for various R/a ratios that represent different substrates. The energy curve corresponding Au(111) is bold and shows binding preferences at 13º, 30º, and 47º in relation to the substrate. **(b)** Predicted adsorption configuration of BPDA on Au(111). Each molecule is at a ± 17º interval from 30º on the Au(111) surface.

The binding energy calculation also provides information on the binding sites of BPDA on fcc(111). Figure 4b represents the three binding configurations of BPDA with the Au(111) surface, which occurs between 0^0 and 60^0, where an energy minimum occurs. In each binding configuration, the phenyl rings sit on the hollow sites on Au(111). The three orientations coexist within the local island in the

electrochemical environment, whereas only a single orientation exists within a local chiral domain in UHV according to the study by Zhu et al. [11].

The ordering is related not only to translational motion, but also to rotational motion, as discussed above. Since we observed island structures in both environments, the translational motion should exist in both cases. This difference suggests that rotational motion for the chiral resolution is feasible in the UHV environment, but not in the electrochemical environment. The energy barrier for rotational motion, shown as cusps between two minima in Figure 4a, should be the same for both UHV and electrochemical environments because it is created by the same interaction between the adsorbate and substrate. This indicates that the existence of a solvent must reduce the intermolecular interactions and thus decrease rotational ability in electrochemical environments. The difference in ordering between the two environments is attributed to the additional interaction between the BPDA molecules and the water solvent in the electrochemical environment. Upon adsorption in UHV, BPDA forms highly stable-ordered islands on Au(111) surface by the intermolecular interactions. Generally, the intermolecular interactions are composed of hydrogen bonds and van der Waals (vdW) interactions. When a BPDA molecule is separated from the assembled structure in UHV, two H-bonds are lost as four hydrogen bonds are shared by two BPDA molecules. Since each H-bond in UHV has energy of about -9 k_BT for room temperature T [35], the H-bond energy difference ΔH is -18 k_BT per molecule between the monomer state and the aggregated state. Boltzmann's constant times the temperature, k_BT, is used as an energy unit in this study for easier comparison between energies. This energy change is sufficient for BPDA molecules to overcome the rotational energy barrier in UHV and thus to form optimal hydrogen bonding by facing each other. The highly ordered chiral resolution in UHV indicates that the difference in H-bond energy is the main driving force in the aggregation formation.

When BPDA molecules are dissolved in water from a solid powder form, each of the molecules is initially hydrogen-bonded together. Upon dissolving, the BPDA forms hydrogen bonds with the surrounding water molecules. This is because the BPDA monomers exist in a protonated form; the pKa of the carboxylic acids is higher than the pH of the electrolyte [36]. The accepted pKa for carboxylic

acids bound to aromatic rings is around 4, or in the case of terephthalic acid 3.54 and 4.34 [37,38]. Since the pH was measured to be 2.1 in the electrochemical cell, which is significantly lower than the expected pKa of the molecule, the protonated state of the carboxylic acid groups is dominant over the deprotonated form. Therefore, four hydrogen bonds are expected to form between water molecules and the carboxylic acid groups of BPDA.

When the BPDA molecules are adsorbed on the Au(111) surface in the electrochemical environment, they formed aggregate structures, which is explained with classic attractive hydrophobic interaction between nonpolar sections of the BPDA molecules surrounded by polar water molecules. The sections attracted each other in such way as to isolate themselves from the molecules. Provided that BPDA can be approximated as a cylindrical shape with a length of l and a radius of r, the total energy is given by $(2\pi rl)\,\gamma_{hydrophobic}/2$, where the division by 2 comes from the fact that only half of the molecule is exposed to water and the other half to the surface. If there are *n* BPDA molecules side by side on the surface, the change of the entropic contribution to the hydrophobic free energy of adsorption ($-T\Delta S$) is estimated to be $n\pi rl\gamma_{hydrophobic}$. The free-energy cost per unit area, $\gamma_{hydrophobic}$, is known to be 7 k_BT/nm^2 due to the presence of hydrophobic molecules [39]. Thus, the entropic contribution to the free energy is estimated to be $-T\Delta S/n \approx -1.6\ k_BT$/molecule for the dimensions of BPDA molecules of l = 1 nm, and r = 0.2 nm obtained with ChemDraw (Cambridge-soft, Cambridge, MA). Therefore, the BPDA molecules coalesce to decrease the hydrophobic surface, which results in positive ΔS.

As found in the length scale of ordered BPDA domains in the FFT analysis, the absence of chiral resolution suggests that the formation of linear networks between BPDA molecules is not energetically favorable due to the mitigated head-to-head hydrogen bonds. The net free energy cost ($E_{head\text{-}head}$) of breaking a single H-bond in water is generally known to be 1-2 k_BT [35]. Simply assuming that the hydrogen bond has a dipole-dipole interaction at an angle (θ) of approximately 120° (in Figure 2a), the hydrogen bond strength ($\Delta H/n$) was estimated to be -0.75 k_BT per molecule in water with the expression of $\Delta H/n = E_{head\text{-}head}\cos\theta$. This estimated value is less than that in UHV by a factor of 10. The effective weakening of hydrogen bonds between BPDA molecules was attributed to the association of water

molecules with adjacent carboxylic acid groups. Overall free energy change ($\Delta G/n$) between the monomer state and the aggregate state is estimated to be $\Delta G/n \approx -2.35\ k_BT$ in water by simply adding $-T\Delta S/n$ and $\Delta H/n$. The negative free energy indicates that the BPDA molecules should form aggregate structures instead of existing as monomers in water by reducing the non-polar sides of BPDA. Due to the involvement of water molecules in intermolecular interactions between BPDA molecules in the electrochemical environment, however, the total energy gain is not sufficient to have chiral resolution with length scale above the molecular size through rotation, although the molecules are able to aggregate on the Au(111) surface.

Conclusions

We studied the effect of a solvent on chiral resolution by investigating the structure of BPDA on Au(111) in an electrochemical environment. The distinctive orientations observed are independent of UHV or electrochemical environments, while the length scales in orientational ordering are dependent on the environment. The same orientations indicate that the interaction between the adsorbate and substrate is the same for both cases. The length scale difference suggests that the effect of the water molecules on intermolecular interactions was the main mechanism behind the absence of chiral resolution of BPDA molecules on a highly symmetric achiral metal surface in the electrochemical environments in comparison to UHV. While the hydrophobic interaction between BPDA molecules leads to the BPDA island structure through an increase in entropy between the monomer and aggregate states, the rotational ability depending on intermolecular interactions is found to be the key factor that determines overall chiral resolution of BPDA on Au(111) in both the UHV and electrochemical environments. These findings contribute to our understanding of two-dimensional stereo-selectivity using chiral surface processes, which potentially could apply to future applications in stereo-selective catalysis.

Acknowledgment. This work is partly supported by the American Chemical Society Petroleum Research Fund (PRF # 47226-GB5), NSF DBI-0852886, NSF DMR-1126854, and Faculty Research Initiative Grants (681A100284) at Boise State University.

References

[1] M. Jacoby, Chem. Eng. News. 82 (2004) 37.

[2] L. C Giancarlo, G.W. Flynn, Acc. Chem. Res. 33 (2000) 491.

[3] M. Mahapatro, C. Gibson, C. Abell, T. Rayment, Ultramicroscopy. 97 (2003) 297.

[4] S. Ahuja, Chiral Separations: Applications and Technology, American Chemical Society, Washington D. C., 1997.

[5] X.Y. Zhao, R.G. Zhao, W.S. Yang, Surf. Sci. 442 (1999) L995-L1000.

[6] E. Mateo Marti, S.M. Barlow, S. Haq, R. Raval, Surf. Sci. 501 (2002) 191.

[7] R.L. Toomes, J.H. Kang, D.P. Woodruff, M. Polcik, M. Kittel, J.T. Hoeft, Surf. Sci. 522 (2003) L9-L14.

[8] B.G. Frederick, Q. Chen, F.M. Leibsle, S.S. Dhesi, N.V. Richardson, Surf. Sci. 394 (1997) 26.

[9] N.M. Santagata, A.M. Lakhani, B.F. Davis, P. Luo, M. Buongiorno Nardelli, T.P.J. Pearl, Phys. Chem. C. 114 (2010) 8917.

[10] B.I. Kim, Langmuir. 22 (2006) 9272.

[11] N. Zhu, T. Osada, T. Komeda, Surf. Sci. 601 (2006) 1789.

[12] N. Katsonis, A. Minoia, T. Kudernac, T. Mutai, H. Xu, H. Uji-i, R. Lazzaroni, S. De Feyter, B.L. Feringa, B. L. J. Am. Chem. Soc. 130 (2008) 386.

[13] T.J. Kristenmacher, G.A. Rand, R.E. Marsh, Acta Crystallogr. B 30 (1974) 2573.

[14] Williams, J. Adsorption and characterisation of chiral amino acids on Cu (110) single crystal surfaces, Ph.D. Thesis, University of Liverpool, 1998.

[15] S.M. Barlow, R. Raval, Surf. Sci. Rep. 50 (2003) 201.

[16] W.D. Xiao, Y.H. Jiang, K. Ait-Mansour, P. Ruffieux, H.J. Gao, R.J. Fasel, Phys. Chem. C. 114 (2010) 6646.

[17] J. Zhang, B. Li, X. Cui, B. Wang, J. Yang, J.G. Hou, J. Am. Chem. Soc. 131 (2009) 5885.

[18] F. Charra, J. Cousty, Phys. Rev. Lett. 80 (1998) 1682.

[19] H. Kimura-Suda, D. Petrovykh, M. Tarlov, L. Whitman, J. Am. Chem. Soc. 125 (2003) 9014.

[20] F. Tao, S. Bernasek, J. Phys. Chem. B. 109 (2005) 6233.

[21] A. Kühnle, T. Linderoth, B. Hammer, F. Besenbacher, Nature. 404 (2002) 891.

[22] Q.H. Yuan, C.J. Yan, H.J. Yan, L. Wan, B. Northrop, H. Jude, P. Stang, J. Am. Chem. Soc. 130 (2009) 8878.

[23] B.-I. Kim, C. Cai, X. Deng, S.S. Perry, Surf. Sci. 538 (2003) 45.

[24] J.V. Barth, J. Weckesser, G. Trimarchi, M. Vladimirova, A. De Vita,C.Z. Cai, H. Brune, P. Gunter, K. Kern, J. Am. Chem. Soc. 124 (2002) 7991.

[25] S. Stepanow, N. Lin, F. Vidal, A. Landa, M. Ruben, J.V. Barth, K. Kern, Nano Letters 5 (2005) 901.

[26] Y.-G. Yan, D. Wang, M.-J. Han, L.-J. Wan, C.-L. Bai, Langmuir. 20 (2004) 7360.

[27] Y.-G. Kim, S.-L. Yan, K. Itaya, Langmuir. 15 (1999) 7810.

[28] Q.-M. Xu, D. Wang, L.-J. Wan, C. Wang, C.-L. Bai, G.-Q. Feng, M.-X. Wang, Langmuir. 18 (2003) 3408.

[29] S. Stepanow, N. Lin, J.V. Barth, K. Kern, J. Phys. Chem. B. 110 (2006) 23472.

[30] M. Lorenzo, C. Baddeley, C. Muryn, R. Ravel, Nature. 404 (2000) 376.

[31] P. Sautet, M.-L. Bocquet, Phys. Rev. B 53 (1996) 4910.

[32] H. Ohtani, R.J. Wilson, S. Chiang, C.M. Mate, Phys. Rev. Lett. 60 (1988) 2398.

[33] C.J. Chen, Introduction to Scanning Tunneling Microscopy, Oxford University Press, New York, 1993, pp. 326.

[34] C. Kittel, Introduction to Solid State Physics, 6th ed., John Wiley & Sons, New York, 1986, pp. 24.

[35] P. Nelson, Biological Physics: Energy, Information, Life; W. H. Freeman and Company, New York, 2004, pp. 273-276.

[36] D. Voet, J. Voet, C. Pratt, Fundamentals of Biochemistry 3rd Edition: Life at the Molecular Level, John Wiley & Sons, New York, 2008, pp. 32.

[37] L.G. Wade, Organic Chemistry, 5th Ed., Pearson Education Inc, Upper Saddle River, New Jersey, 2003, pp. 1219.

[38] D.R. Lide, CRC Manual of Chemistry and Physics, 85th Ed., CRC Press, New York, 8, 2004-2005, 53.

[39] R. Phillips, Physical Biology of the Cell, Garland Science, New York, 2009, pp. 201-204.